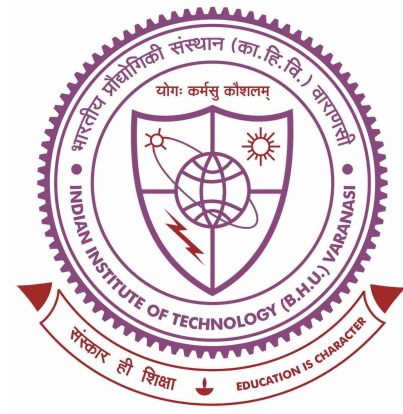


# Self-assembly of Polymer Fluids Under External Stimuli



*Thesis submitted in fulfilment  
for the Award of  
**Doctor of Philosophy**  
in  
**Physics***

*by*  
**Ashish Kumar Singh**

**Department of Physics  
Indian Institute of Technology  
Banaras Hindu University  
Varanasi - 221005, India**

Roll No.  
19171023

Year of Submission  
06 August 2024

*To my loving parents and Nanaji.*

## Certificate

It is certified that the work in the thesis titled **Self-assembly of Polymer Fluids Under External Stimuli** by Mr. Ashish Kumar Singh, Roll Number 19171023, has been carried out under my supervision, and this work has not been submitted elsewhere for a degree.

*Awaneesh Singh*

Signature:

Dr. Awaneesh Singh

Assistant Professor

Department of Physics

Indian Institute of Technology (BHU)

Varanasi, India - 221005

**Assistant Professor**

**Department of Physics**

**Indian Institute of Technology**

**(Banaras Hindu University,**

**Varanasi-221005**

## Declaration

I, **Ashish Kumar Singh**, certify that the work embodied in this thesis is my own bona-fide work and carried out by me under the supervision of **Dr. Awaneesh Singh** from 29 July-2019 to 06 August-2024 at the **Department of Physics**, Indian Institute of Technology (BHU), Varanasi. The matter embodied in this thesis has not been submitted for the award of any other degree/diploma. I declare that I have faithfully acknowledged and given credits to the research workers whenever and wherever their works have been cited in my work in this thesis. I further declare that I have not wilfully copied any others' work, paragraphs, text, data, results, etc., reported in journals, books, magazines, reports dissertations, theses, etc., or available at websites and have not included them in this thesis and have not cited as my own work.

Date: 06-Aug.-2024

Signature

Place: Varanasi

Ashish Kumar Singh

## Certificate by the Supervisor

It is certified that the above statement made by the student is correct to the best of my knowledge.

Awaneesh Singh

Signature:

Dr. Awaneesh Singh

Assistant Professor

**Assistant Professor**

**Department of Physics**

**Indian Institute of Technology**

**(Banaras Hindu University)**

**Varanasi-221005**

Signature of the Head of the Department

Dr. Sandip Chattarjee

Professor

Department of Physics, IIT (BHU)

HEAD/विभागाध्यक्ष

भौतिकी विभाग / Deptt. of Physics

आ0प्रौ0सं0/(का0हि0वि0)/IIT (BHU)

वाराणसी / Varanasi-221005

## Copyright Transfer Certificate

Title of the Thesis : Self-assembly of Polymer Fluids Under External Stimuli

Name of the Student : Ashish Kumar Singh

### Copyright Transfer

The undersigned hereby assigns to the Indian Institute of Technology (Banaras Hindu University) Varanasi all rights under copyright that may exist in and for the above thesis submitted for the award of the **Doctor of Philosophy in Physics**.

Date 06-Aug-2024

Signature

Place Varanasi

Ashish Kumar Singh

**Note:** However, the author may reproduce or authorize others to reproduce material extracted verbatim from the thesis or derivative of the thesis for author's personal use provided that the source and the Institute's copyright notice are indicated.

# Acknowledgements

I would like to express my gratitude to everyone who has helped and supported me throughout my PhD journey.

Above all, I wish to express my sincere gratitude to my PhD supervisor, Dr. Awaneesh Singh, for his unwavering support throughout my PhD journey. He consistently guided me from the basics of statistical mechanics and introduced me to an intriguing and challenging research topic. His expertise and experience were invaluable in helping me to solve various research problems, which have numerous practical applications and personal issues. I also appreciate his tireless efforts in patiently revising multiple drafts of my papers and thesis.

I want to express my deep admiration for Prof. Sanjay Puri (School of Physical Sciences, Jawaharlal Nehru University, New Delhi), for our collaboration on photo-induced bond-breaking. His deep understanding of statistics and mathematical physics has been incredibly helpful to me. Working with him has been an enriching experience, significantly advancing my understanding of new concepts and the visualization of research results.

I am sincerely grateful to all the faculty members of our department for their consistent cooperation and support during my Ph.D. days. I extend special thanks to the head of the department, Prof. Sandip Chatterjee, for his outstanding support. I also wish to express my gratitude to my RPEC committee members, Dr. Shradha Mishra (Department of Physics, IIT (BHU)) and Dr. Lavanya Selvaganesh (Department of Mathematics, IIT (BHU)), for their invaluable guidance and feedback throughout my studies and thesis completion. Additionally, I appreciate the assistance and support provided by all non-teaching staff members for their help with various administrative tasks.

I am grateful to acknowledge the financial support by the Council for Scientific and Industrial Research (CSIR), India, through a research fellowship. I also thank to Param Shivay and C.C.I.S., IIT (BHU) for providing me the computational facilities.

I enjoyed my Ph.D. days at BHU with the company of friends who were always ready to help with both academic and non-academic issues. Pawan always helped me from the beginning, mainly when we were modeling the code for Monte Carlo simulations. Samiksha was always willing to discuss fundamental concepts and model new problems. She also supported me with both personal and professional challenges. During our Ph.D., we had many fantastic days together and shared lots of wonderful experiences. I would also like to thank all my friends and batchmates. To all the labmates Avinash, Samiksha, Devendra, Vanshika, and Ankita, thank you for providing such an enjoyable and productive working environment. I spent pleasant days with Devendra and Avinash in our flat. Special thanks to Anish for bringing delicious food from Rajasthan Sweets and cooking tasty meals for us with refreshing non-academic discussions. I must acknowledge my childhood friends Saurabh, Vikash, Ankit, Harsh, and Vivek for always helping me with all academic and personal matters and creating a joyful environment around me.

I have no words to adequately describe the contribution of my family members, who have always stood by my side in all my endeavors. I sincerely acknowledge the unwavering love of my parents, their constant encouragement, and their unconditional support throughout this journey. I also acknowledge the support and care of my Didi, Jiju, Bhai, and Bhabhi. I am also grateful to my Nanaji, who always supported me and provided valuable feedback on my decisions.

Finally, my best friend Pooja deserves special recognition for her love and care. I appreciate her for every academic and non-academic discussion and her invaluable feedback. I am grateful for her patience in listening to all my non-academic conversations and unwavering support.

# Publications

1. Photo-induced bond breaking during phase separation kinetics of block copolymer melts- A dissipative particle dynamics study; Ashish Kumar Singh, Avinash Chauhan, Sanjay Puri, Awaneesh Singh; *Soft Matter*, 17 (7), 1802-1813 (2021).
2. Phase separation kinetics of block copolymer melts confined under moving parallel walls: A DPD study; Ashish Kumar Singh, Awaneesh Singh, *Computational Materials Science*, 226, 112224 (2023).
3. Growth kinetics and morphology characterization of binary polymeric fluid under random photo illumination; Ashish Kumar Singh, Avinash Chauhan, Awaneesh Singh; *Journal of Chemical Physics*, 160, 024907 (2024).
4. Photomodulated phase-separation kinetics of block copolymer melts: A DPD Simulation Study; Avinash Chauhan, Ashish Kumar Singh, Awaneesh Singh; *Molecular Simulation*, 50(5), 394-403 (2024).
5. DPD simulation study of segregation kinetics of binary polymer fluids: effect of external shear; Ashish Kumar Singh, Samiksha Shrivastav, Awaneesh Singh (*manuscript in preperation*).
6. Effect of random photo illumination on phase-separating dimers: A DPD simulation study; Ashish Kumar Singh, Awaneesh Singh (*work in progress*).
7. Insights into phase separation kinetics of fluids within polymer gel; Ashish Kumar Singh, Awaneesh Singh (*work in progress*).

8. Mixing and demixing of dimer melt system under the effect of alternate light cycles and shear: Ashish Kumar Singh, Vanshika Saini, Awaneesh Singh (*work in progress*).
  
9. Phase separation kinetics of miktoarm star polymers in a solvent: Effect of size and number of arms; Devendra Kumar Verma, Ashish Kumar Singh, Avinash Chauhan, Awaneesh Singh (*work in progress*).

# Abstract

We have studied the phase separation kinetics of polymer fluids using the dissipative particle dynamics (DPD) simulation. In chapter 1, we have discussed the basic concepts on phase separating binary (AB) fluids, including the fundamental observables required to characterize the evolution morphology. We have explored mainly the following systems, simple binary fluid, polymer blend, and block copolymer (BCP) melt. The fundamental concepts of DPD simulation are also discussed, including the potential energies and details of simulation parameters used in further chapters.

In Chapter 2, we examine the phase segregation of a BCP melt system in  $3d$  under external stimuli such as light. The bonds joining incompatible beads in BCP chains are considered photo-sensitive. We start with a homogeneous system and rapidly quench it to a temperature  $T < T_c$ , where  $T_c$  is the critical temperature. Simultaneously, we apply alternating on- and off-light cycles to the system. During the on-light cycles, bond-breaking reactions of the photo-sensitive bonds generates two corresponding active radicals. These active beads undergo recombination reactions in off-cycles, regenerating the original BCP chains. During the on-light cycles, macrophase separation occurs due to the breaking of stimuli-sensitive bonds, causing the two blocks to separate and behave as polymer blends. Conversely, off-light cycles result in microphase separation due to bond constraints between incompatible blocks. The study is divided into two sets: set 1 begins with an off-light cycle, while set 2 starts with an on-light cycle. We monitor domain evolution, scaling functions, and growth laws during each cycle. The characteristic length scale follows a power law growth  $R(t) \sim t^\phi$ , where  $\phi$  is the growth exponent. Our simulation shows that the length scale follows all three regimes: diffusive ( $\phi \sim 1/3$ ), viscous hydrodynamic ( $\phi \sim 1$ ), and inertial hydrodynamic ( $\phi \sim 2/3$ ) growth.

The time variation of the number of bonds broken and recombined demonstrates that our model accurately reproduces the first-order kinetics of photo-sensitive reactions.

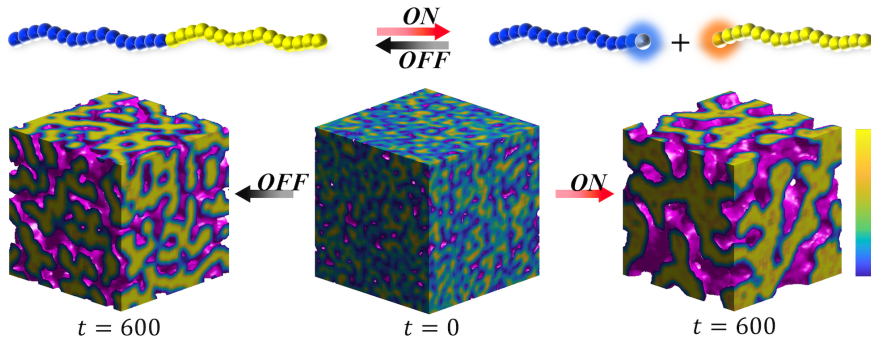


Fig. 1: Effect of on- and off-light cycles on the phase separation kinetics of BCP melt systems.

In chapter 3, we further explore the phase separation kinetics of polymer fluids using DPD simulations. We apply random photo-illumination to study its impact on the evolution of polymer blend and BCP melt systems. The polymer blend system has active radicals at one end of its each chain, while the BCP melt has light-sensitive bonds joining the incompatible blocks. The initial homogeneous mixture is quenched to a temperature below its critical value to induce phase separation. Simultaneously, the system is exposed to random photo-illumination, leading to two concurrent random events: (a) bond recombination reactions of the active radicals during the off-state of light and (b) breaking of photo-sensitive bonds in BCP chains when the light is on. The variation in the intensity of illuminated light is simulated by adjusting the bond-breaking probability  $P_b$ . The characteristic domain growth follows the typical power-law behavior  $R(t) \sim t^\phi$ . With varying  $P_b$ , the length scale transitions from microphase to macrophase separation at specific transition probabilities for both systems. The bond recombination probability is set to its maximum value  $P_c = 1$ , making microphase separation kinetics dominant at low  $P_b$  values. The excellent overlap in scaling function data indicates the formation of statistically similar domains across all probabilities. This study enhances

the understanding of phase separation kinetics in polymer fluids under external stimuli, affecting the fundamental properties of the system.

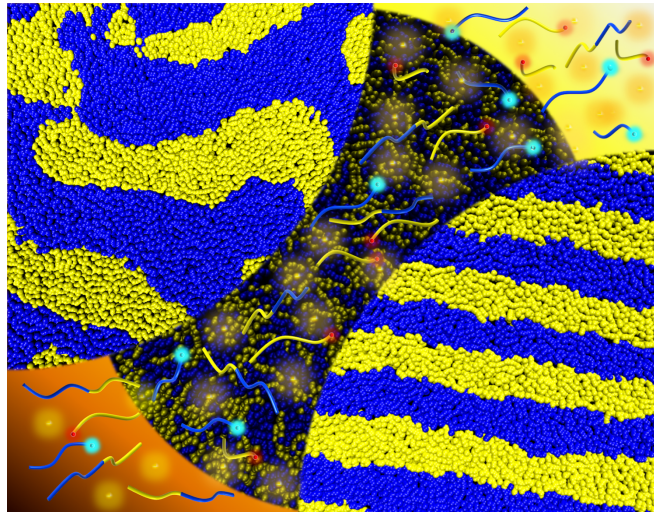


Fig. 2: Random photo-illumination on polymer blend systems.

In Chapter 4, we investigate the effect of external shear on the phase separation kinetics of BCP melt system. We consider a critical diblock copolymer melt system confined along the  $z$ -direction between two parallel solid walls at the top and bottom of the system. Initially, we quench the homogeneous mixture to a very low temperature and simultaneously apply external shear by moving the walls in specific directions. Our study is divided into four scenarios based on wall motion: (i) Both walls are fixed, (ii) Only the top wall moves with a constant velocity in  $x$ -direction, (iii) Both walls move in the same  $x$ -direction with the same velocity, (iv) The top wall moves in  $x$ -direction, while the bottom wall moves in opposite direction. We monitor the effect of external shear on domain coarsening, scaling functions, growth laws, anisotropy, and other relevant parameters. The characteristic length scale follows the usual power law behavior with diffusive growth at the early stage, which saturates at late times. However, with the application of shear, significant deviations are observed in the length scale data due to the formation of well-ordered structures. To minimize the effect of shear, domains rearrange themselves in a particular direction. Consequently, lamellar morphology forms much

earlier than in typical BCP melt systems, especially in scenario (iv), where a well-ordered lamellar structure is observed within specified time intervals. The viscosity plot shows shear-thinning behavior upon the application of shear for all cases. Overall, our study highlights the influence of shear rates on the microphase separation kinetics of BCP melts.

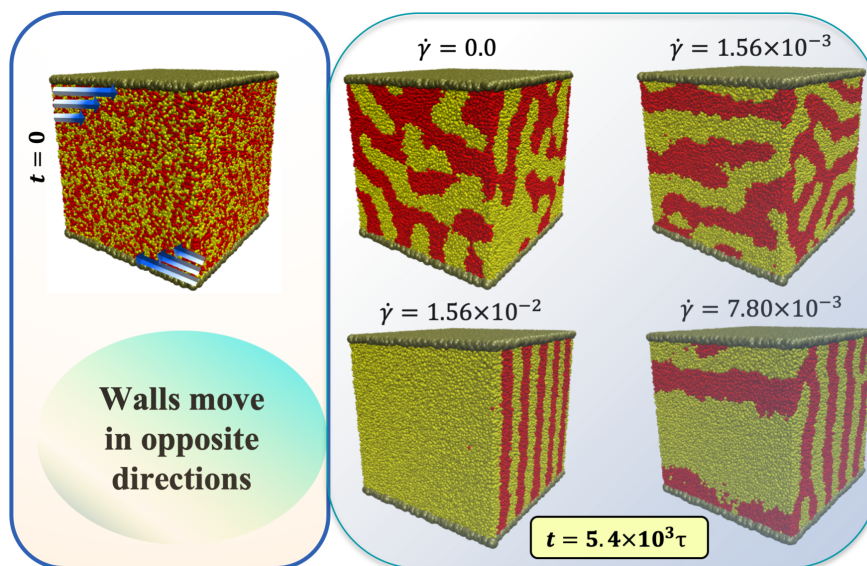


Fig. 3: Effect of external shear on the phase separation kinetics of BCP melts.

In Chapter 5, we examine the phase separation kinetics of a polymer blend system under the application of external shear. This study explores the effects of shear on both critical and off-critical polymer blend systems. Two rigid walls are placed at the top and bottom of the system, and shear is applied by moving these walls in specific directions. We again explored the four scenarios related to the shear generated by the wall motion, as expressed earlier for chapter 4. We monitor the effect of external shear on various properties such as morphological evolution, scaling functions, domain growth, radial distribution function, velocity profile, and viscosity. To counteract the effect of shear, the domains rearrange in a particular direction, forming organized structures. The characteristic length scale follows the typical power-law behavior:  $R(t) \sim t^\phi$ , where  $\phi$  is the effective growth exponent. Initially, the length scale exhibits viscous hydrodynamic

growth ( $\phi \sim 1$ ), transitioning to inertial hydrodynamic growth ( $\phi \sim 2/3$ ) later on. At high shear rates, we observe anisotropy in the system due to domain flow in the direction of shear, resulting in more stable structures. As the shear rate increases, shear viscosity decreases, indicating shear-thinning behavior in all cases. In the off-critical mixture (case 4: when both walls are moving in opposite directions), cylindrical domains form at high shear rates, this is not observed in other cases within the same time interval. This study provides insights into how shear influences phase separation kinetics and domain organization in polymer blend systems.

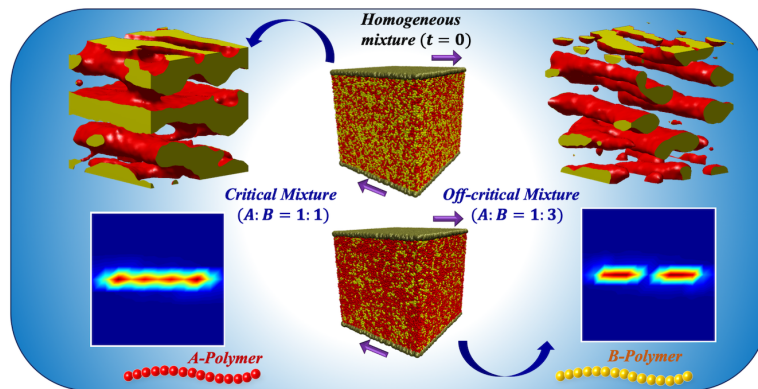


Fig. 4: Impact of external shear on critical and off-critical polymer blend systems.

# Table of contents

List of figures	xix
List of publications	xxxv
<b>1 Introduction</b>	<b>1</b>
1.1 Kinetics of phase transition . . . . .	1
1.1.1 Liquid-liquid unmixing . . . . .	3
1.2 Characterization of domain evolution and growth laws . . . . .	7
1.2.1 Radial distribution function . . . . .	8
1.2.2 Local number density distribution . . . . .	9
1.2.3 Correlation function and the structure factor . . . . .	9
1.2.4 Average domain length and growth laws . . . . .	11
1.3 General examples of phase separating systems . . . . .	16
1.3.1 Binary simple fluid . . . . .	17
1.3.2 Binary polymer blend . . . . .	19
1.3.3 Block copolymer melt . . . . .	21
1.4 DPD simulation method . . . . .	23
1.4.1 Modeling polymer chains . . . . .	26
1.4.2 Updates in position and velocity . . . . .	27
1.4.3 Model parameters . . . . .	28

---

1.5	Overview of the thesis . . . . .	29
1.6	Summary and discussion . . . . .	31
<b>2</b>	<b>Phase separation kinetics of BCP melts under on-off light cycles</b>	<b>33</b>
2.1	Introduction . . . . .	33
2.2	Photo-controlled reactions mechanism . . . . .	36
2.3	System details . . . . .	37
2.4	Effect of alternate light cycles . . . . .	38
2.4.1	Reaction kinetics . . . . .	41
2.4.2	Quantitative study of evolution . . . . .	43
2.4.3	Characterization functions . . . . .	45
2.4.4	Growth laws . . . . .	48
2.5	Summary and discussion . . . . .	50
<b>3</b>	<b>Random photo-illumination on segregating polymeric fluids</b>	<b>53</b>
3.1	Introduction . . . . .	53
3.2	Modeling random photo-illumination . . . . .	55
3.3	System details . . . . .	56
3.4	Polymer blend system . . . . .	57
3.4.1	Domain morphology and reaction kinetics . . . . .	57
3.4.2	Radial distribution function . . . . .	60
3.4.3	Characterization functions and anisotropy . . . . .	61
3.4.4	Growth laws . . . . .	64
3.5	BCP melt system . . . . .	66
3.5.1	Domain morphology and reaction kinetics . . . . .	67
3.5.2	Characterization functions . . . . .	69
3.5.3	Growth laws . . . . .	71

---

3.6	Summary and discussion . . . . .	73
<b>4</b>	<b>Block copolymer melts confined under moving parallel walls</b>	<b>75</b>
4.1	Introduction . . . . .	75
4.2	System details . . . . .	78
4.3	Calculation of velocity profile and shear-viscosity . . . . .	79
4.4	Anisotropy parameter . . . . .	80
4.5	Effect of external shear on viscosity and velocity profile . . . . .	81
4.5.1	Velocity profile depends on different parameters . . . . .	82
4.6	Average bond length and instantaneous temperature . . . . .	86
4.7	Case 1: Both walls fixed . . . . .	87
4.7.1	RDF and density distribution . . . . .	88
4.7.2	Characterization functions . . . . .	89
4.8	Case 2: Only top wall moves . . . . .	91
4.8.1	RDF and density distribution . . . . .	92
4.8.2	Characterization functions . . . . .	94
4.9	Case 3: Both walls move in the same direction . . . . .	96
4.9.1	RDF and density distribution . . . . .	97
4.9.2	Characterization functions . . . . .	98
4.9.3	Anisotropy developed in case 2 and case 3 . . . . .	100
4.10	Case 4: Both walls move in opposite directions . . . . .	101
4.10.1	Characterization of domain coarsening . . . . .	102
4.10.2	Anisotropy for different shear rates . . . . .	105
4.11	BCP melt system with smaller chain length . . . . .	108
4.12	Effect of shear on asymmetric BCP melt system . . . . .	110
4.13	Summary and discussion . . . . .	113

---

<b>5</b>	<b>Segregation kinetics of binary polymer fluids: effect of external shear</b>	<b>116</b>
5.1	Introduction . . . . .	116
5.2	System details . . . . .	119
5.3	Critical mixture of polymer blend . . . . .	120
5.3.1	Case 1: Both walls fixed . . . . .	123
5.3.2	Case 2: Only top wall moves . . . . .	125
5.3.3	Case 3: Both walls move in the same direction . . . . .	127
5.3.4	Case 4: Both walls move in opposite directions . . . . .	128
5.4	Off-critical mixture of polymer blend . . . . .	133
5.4.1	Case 1: Both walls fixed . . . . .	133
5.4.2	Case 2: Only top wall moves . . . . .	135
5.4.3	Case 3: Both walls move in the same direction . . . . .	137
5.4.4	Case 4: Both walls move in opposite directions . . . . .	138
5.5	Summary and discussion . . . . .	142
<b>6</b>	<b>Conclusion and future plan</b>	<b>144</b>
6.1	Conclusion . . . . .	144
6.2	Future Plan . . . . .	146
	<b>References</b>	<b>148</b>

# List of figures

- 1 Effect of on- and off-light cycles on the phase separation kinetics of BCP melt systems. . . . . xi
- 2 Random photo-illumination on polymer blend systems. . . . . xii
- 3 Effect of external shear on the phase separation kinetics of BCP melts. . . . . xiii
- 4 Impact of external shear on critical and off-critical polymer blend systems. . . . . xiv
  
- 1.1 Phase diagram for ferromagnet [1]. Here  $T$  and  $h$  represents the temperature and the magnetic field, respectively. The line ( $T < T_c, h = 0$ ) denotes the first-order transition, and the point ( $T_c, h_c = 0$ ) signifies the second-order critical point. When  $T > T_c$ , the system is in a disordered state, whereas for  $T < T_c$ , it falls in magnetized state with spins aligned either upwards or downwards. . . . . 3
- 1.2 Phase diagram for (AB) binary mixture [1].  $\phi$  depict the volume fraction and  $T$  represents the temperature. At the second-order critical point,  $T/T_c = 1$ , and  $\phi = 0.5$ . A solid line represents the coexistence curve. The system is in the homogeneously mixed state above the coexistence curve and starts the phase separating below it. The dashed line is a spinodal curve representing the metastable states between spinodal and coexistence curves. . . . . 6

1.3	(a) Schematic for calculating RDF at a distance $r$ from the reference particle. (b) The general behavior of RDF representing the distribution of $B$ -type particles around $A$ in binary fluids. . . . .	8
1.4	Plots for the correlation function and corresponding structure factor curves for binary mixture are shown in (a) and (b), respectively. The black dashed line in (b) with a slope of $-4$ represents the Porod's tail in $3d$ . . . . .	11
1.5	Schematic represents the repeating units of simple fluids, polymer blends, and block copolymer melts. . . . .	16
1.6	(a-e) The evolution morphology of phase separating binary fluid at different time intervals, indicated alongside each image. (f) $g_{AB}(r)$ vs. $r$ for different time intervals. . . . .	17
1.7	(a) Plots for $C(r, t)$ vs. $r/R(t)$ . (b) The structure factor $S(k, t)$ vs. $kR(t)$ at various time intervals, as indicated in the legends. The solid black line represents the porod's tail as $k \rightarrow \infty$ . Inset of (a) and (b) plot the unscaled correlation and structure factor. (c) $R(t)$ vs. $t$ for a simple fluid. Solid lines, characterized by slopes of 1 and $2/3$ , signify the phases of viscous and inertial hydrodynamic growth experienced by the system. . .	19
1.8	We plot the evolved morphology of the polymer blend system in (a-e) at different time intervals. (f) plots the corresponding RDF curves. . . . .	20
1.9	In (a) and (b), we depict the scaled $C(r, t)$ vs. $r/R(t)$ and $S(k, t)$ vs. $kR(t)$ , respectively, for different time intervals as indicated in the legends. Inset of (a) and (b) plot the unscaled correlation and structure factor. (c) The time-dependent behavior of $R(t)$ . . . . .	21
1.10	In (a-e), snapshots of the domain morphology of the BCP melt system are shown at various time intervals. Corresponding RDF plots are depicted in (f). . . . .	22

- 
- 1.11 In correspondence to the evolved morphology displayed in Fig. 1.10, we plot the unscaled and scaled correlation function in (a) and (b), respectively. (c) and (d) represent the unscaled and scaled structure factor. . . . . 23
- 1.12 Temporal variation of characteristic length scale  $R(t)$  vs.  $t$ . . . . . 24
- 2.1 (a) Schematic of bond-breaking and combination reactions during the on- and off-light cycles.  $P_b$  and  $P_c$  depict the probability of bond-breaking and recombination reactions. (b) The homogeneous mixture of BCP melt system (1 : 1 ratio of  $A$  and  $B$ -type beads: critical composition) after the equilibration. (c) Representation of color marks of the beads: Inactive  $A$  and  $B$ -type beads are represented by blue and yellow. At the same time, the corresponding active radicals are shown with glowing cyan and glowing orange. . . . . 37
- 2.2 (a) Homogeneous mixture of BCP ( $A_nB_n; n = 16$ ) melt at  $t = 0$ . (b-f) Subsequent snapshots depict the evolution after each cycle in a sequence of off  $\rightarrow$  on  $\rightarrow$  off  $\rightarrow$  on  $\rightarrow$  off. The blue and yellow colors represent the  $A$  and  $B$ -type beads, respectively. . . . . 39
- 2.3 Evolution snapshots for set 1 after the first and second cycles at different bond-breaking probabilities: (a)  $P_b = 0.1$ , (b)  $P_b = 0.5$ , and (c)  $P_b = 1.0$ . The first column depicts the microphase-separated structures at  $t = 600$ . The second column shows the snapshots after cycle 2. The interface between  $A$  and  $B$ -type domains is illustrated in the third column at  $t = 1200$ . 40

- 2.4 Evolution snapshots for set 2 after the completion of cycle 1 (on) and cycle 2 (off) at different bond-breaking probabilities: (a)  $P_b = 0.1$ , (b)  $P_b = 0.5$ , and (c)  $P_b = 1.0$ . The first column shows the macrophase-separated evolution morphology at  $t = 600$ . The second column displays the snapshots after cycle two. The interface between A and B-type domains is illustrated in the third column, corresponding to snapshots shown in column two. . . . . 40
- 2.5 We normalize the cumulative number of bonds broken ( $N_b$ ) during on-cycles and a cumulative number of bonds recombined ( $N_c$ ) during off-cycles by the total number of photo-sensitive bonds  $N_{pc}$  at  $t = 0$ . Corresponding normalized numbers are denoted by  $n_b$  and  $n_c$ , respectively, and plotted as a function of time. (a) Plots for  $n_b$  vs.  $t$  during on-cycles and  $n_c$  vs.  $t$  during off-cycles of set 1. (b) Variation of  $n_b$  with time for different  $P_b$  values for cycle 2 in set 1. (c) Time variation of  $n_b$  and  $n_c$  corresponding to different cycles of set 2 is plotted with different symbol types. The dashed lines represent the exponential fits,  $n_b(t) \sim (1 - e^{-\lambda P_b t})$  followed by each plot, where  $\lambda$  is the fitting parameter. . . . . 42
- 2.6 (a) Plots for radial distribution function  $g_{AB}(r)$  vs.  $r$  after each cycle of set 1. (b) Local number density distribution of A-type beads along  $z$ -direction for the same data set plotted in (a) with various symbol types. For each plot, the probability  $P_b$  and  $P_c$  are fixed at 1.0. . . . . 43
- 2.7 Comparison of  $g_{AB}(r)$  vs.  $r$  for different probabilities in cycle 2 (on-cycle) of set 1. The inset plot shows the RDF for cycle 4 (on-cycle) with different  $P_b$  values indicated by different symbols as specified in the legends. . . . 44

- 2.8 (a) and (b) plots the spherically averaged scaled correlation function and corresponding structure factor after the completion of different on- and off-light cycles in set 1. Various symbol types represent the data at different time intervals. The solid line in (a) depicts the zero crossing of the correlation function. The tail of the structure factor follows Porod's law, illustrated with a solid black line in (b) with slope  $-4$ . (c-d) Scaled correlation function  $C(r, t)$  vs.  $r/R(t)$  and the structure factor  $S(k, t)$  vs.  $kR(t)$  for different time intervals in cycle 2 set 1 (light-on). (e-f) Same set of observables plotted in (c) and (d) for cycle 3 set 1 (light-off). . . . . 46
- 2.9 (a-b) Scaled correlation and structure factor after ending each light cycle for set 2. Various symbol types represent the different time intervals. (c-d) Plots for  $C(r, t)$  vs.  $r/R(t)$  and  $S(k, t)$  vs.  $kR(t)$  for the evolution through cycle 1 set 2 (bond-breaking on). (e-f) Same set of observables as in (c) and (d) for the evolution through cycle 2 set 2 (bonds are recombining). 47
- 2.10 (a) Average domain size  $R(t)$  vs.  $t$  is plotted for microscopic domain growth during off-cycles (1, 3, and 5) of set 1 when bond recombination reactions reform the BCP chains. A solid black line represents the expected diffusive growth ( $\phi \sim 1/3$ ) at early times. (b) Plots for average length scale  $R(t)$  vs.  $t$  during macroscopic domain growth in cycles 2 and 4, when bond-breaking reactions turn the BCP melt system into a binary polymer blend. The solid line displays the inertial hydrodynamic growth ( $\phi \sim 2/3$ ) for  $d = 3$  fluids. . . . . 49
- 2.11 Logarithmic plots for the average domain growth  $R(t)$  as a function of time. Data corresponding to on-cycles (1, 3, and 5) of set 2 are plotted in (a) while (b) plots the data for off-cycles (2 and 4). Solid lines represent the growth laws followed by the system in different cycles. . . . . 50

- 
- 3.1 Schematic of bond-breaking and combination reactions under random photo-illumination. The inactive  $A$  and  $B$ -type beads are represented by blue and yellow. At the same time, the corresponding active radicals are shown with glowing cyan and glowing orange. . . . . 56
- 3.2 (a-d) Domain evolution snapshots of polymer blend system for different bond breaking probabilities at  $t = 3.0 \times 10^3$ . Blue and yellow colors represent  $A$  and  $B$  beads, respectively. (e) Time variation of the normalized cumulative number of bonds broken ( $n_b$ ) at various  $P_b$  values. (f)  $n_b$  vs.  $P_b$  at two different time intervals  $t = 2.0 \times 10^2$  and  $3.0 \times 10^3$  plotted with black and red curves, respectively. Inset plots the  $n_b$  vs  $P_b$  on log-log scale at higher  $P_b$  values. (g) Scaling of the normalized cumulative number of bonds broken at low  $P_b$  values ( $0.01 - 0.1$ ). Corresponding scaled data is denoted as  $n_{bs}$ . The scaling at higher  $P_b$  values ( $0.2 - 1.0$ ) is shown in (h). Legends at the top represent the different  $P_b$  values depicted with various symbol types. . . . . 58
- 3.3 (a) Radial distribution function,  $g_{AB}(r)$ , at  $P_b = 0.5$ . Different symbol types in the legends represent different time intervals. (b) Comparison of  $g_{AB}(r)$  vs,  $r$  at different  $P_b$  values at a late time  $t = 3.0 \times 10^3$ . . . . . 60
- 3.4 Spherically averaged scaled correlation function  $C(r, t)$  vs.  $r/R(t)$  at different time intervals are plotted with different symbols at  $P_b = 0.01$  in (a) and  $P_b = 0.5$  in (b). The solid black line represents the zero-crossing. 61

- 3.5 (a-b) Scaled correlation function  $C(r, t)$  vs.  $r/R(t)$  for different bond-breaking probability  $P_b = 0.01, 0.1, 0.5,$  and  $1.0$  plotted with black, red, green, and blue curves respectively for  $t = 1.2 \times 10^3$  in (a), and  $t = 3.0 \times 10^3$  in (b). Corresponding evolved morphologies are displayed in Figs. 3.2(a)-3.2(d). (c-d) Plots for the structure factor along  $x, y,$  and  $z$  direction at  $t = 3.0 \times 10^3$  are displayed in (c) for  $P_b = 0.01$  and (d) for  $P_b = 0.5$  to discuss the anisotropy developed within the system. . . . . 63
- 3.6 (a) The characteristic length scale  $R(t)$  vs.  $t$  for different bond-breaking probabilities  $P_b \in (0.0, 1.0)$  at a fixed bond recombination probability  $P_c = 1.0$ . The solid lines represent the growth laws followed by the system ( $1/3$  for the diffusive growth and  $2/3$  for the inertial hydrodynamic growth). For a reference case, the length scale of pure BCP melt and pure polymer blend is plotted with the black and magenta curves. (b) Plots for  $R(t)$  vs.  $P_b$  at different time intervals are depicted with various symbol types in the legends. (c)  $\phi_{eff}$  vs.  $1/t$  for different bond-breaking probabilities plotted with various symbols given in the legends. . . . . 65
- 3.7 (a-d) Domain evolution of BCP melt system at different light intensities: ( $P_b = 0.01, 0.1, 0.5,$  and  $1.0$ ) at  $t = 1.2 \times 10^4$ . (e) Time-dependent behavior of  $n_b$  at different bond-breaking probabilities. (f)  $n_b$  vs.  $P_b$  at two different time intervals:  $t = 1.2 \times 10^3$  (black curve) and  $t = 1.2 \times 10^4$  (red curve). Inset plots the data at high  $P_b$  values representing the power law growth. (g) and (h) plot the  $n_b$  vs.  $t$  data after scaling with the power law equation with the unit and lower growth exponents, respectively. . . . . 67

- 3.8 (a-b) Comparison of the scaled correlation function and structure factor for  $P_b = 0.01$  at various time intervals, depicted by different symbols. In (a),  $C(r, t)$  vs.  $r/R(t)$  curves are plotted on a linear scale, while (b) shows  $S(k, t)$  vs.  $kR(t)$  on a logarithmic scale. (c-d) The same quantities are plotted for  $P_b = 0.5$ . . . . . 69
- 3.9 (a-b) Comparison of the correlation and the structure factor curves for different bond-breaking probabilities  $P_b$ : 0.01 (black), 0.1 (red), 0.5 (green), and 1.0 (blue), at a late-time regime,  $t = 1.2 \times 10^4$ . . . . . 70
- 3.10 (a) The characteristic domain size,  $R(t)$  vs.  $t$  on a logarithmic scale for various  $P_b$  values. The length scale for a pure BCP melt system is plotted with a black dashed curve for a reference case. The inset of (a) represents the plots for  $R(t)$  vs.  $P_b$  at different time intervals indicated by various symbol types in the legends. (b) The effective growth exponent,  $\phi_{eff}$  is plotted as a function of  $1/t$  corresponding to the length scale presented in (a). . . . . 72
- 4.1 (a) Plots of the average velocity profile,  $\langle v_x \rangle$  vs.  $z$ , at a high shear rate ( $\dot{\gamma} = 1.56 \times 10^{-2}$ ), with different symbols representing the various scenarios. (b) Plots of shear viscosity,  $\langle \eta \rangle$ , vs.  $\dot{\gamma}$  at the late time step ( $t = 5 \times 10^3$ ) for all three scenarios, each indicated by distinct symbols. . . . . 81

- 4.2 (a-c) Plots for the velocity profile,  $\langle v_x \rangle$  along  $z$ -direction. (a)  $\langle v_x \rangle$  vs.  $z$  at different shear rates mentioned in the legend at a fixed chain length,  $N_p = 32$ . (b) Effect of BCP chain length on  $\langle v_x \rangle$  vs.  $z$  at a fixed shear rate,  $\dot{\gamma} = 1.56 \times 10^{-2}$ . The three black, red, and green curves represent the data for chain length  $N_p = 8, 16,$  and  $32$ , respectively. In (a) and (b), The height of the box is fixed at  $L = 64$  in a cubic simulation box. We vary the height of the box in (c) and compare the velocity profile by keeping the box length ( $L = 64$ ) fixed in  $x$ - and  $y$ -directions at  $\dot{\gamma} = 1.56 \times 10^{-2}$  and  $N_p = 32$ . In (d-f), the velocity profiles are plotted for case 3 with the variation of the same set of parameters as discussed in (a-c). . . . . 83
- 4.3 Plots for average velocity profile against time for all three cases of applied shear are mentioned at the top. (a-c) Plots for  $\langle v_x \rangle$  vs.  $t$  for different shear rates mentioned in the legends. Data is taken at a plane near the top wall. In (d-f)  $\langle v_x \rangle$  is plotted at different  $xy$ -planes for a moderate shear rate  $\dot{\gamma} = 7.8 \times 10^{-3}$ . (g-i) plots the same data set as in (d-f), for high shear rate  $\dot{\gamma} = 1.56 \times 10^{-2}$ . . . . . 85
- 4.4 (a), (c), and (e) represent the time-dependent average bond length  $\langle l_b \rangle$  for cases 2-4 mentioned at extreme right. Various symbols in the legends represent the different shear rates applied to the system. In the second column (b), (d), and (f), we plotted the instantaneous temperature over time for the same cases as in the first column. . . . . 86
- 4.5 Comparison of late stage morphology of phase separating critical BCP melt for (a)  $N_p = 8$ , (b)  $N_p = 16$ , and (c)  $N_p = 32$ . The second right frame shows the corresponding isosurfaces. . . . . 87

- 4.6 (a) Plots for the radial distribution function  $g_{AB}(r)$  vs.  $r$  for BCP chain length  $N_p = 32$  for case 1. Different symbols types mentioned in the legends represent the various time intervals. (b) Average number density distribution function  $\rho_A(y)$  vs.  $y$  of  $A$ -type beads, corresponding to the same time intervals as in (a). . . . . 89
- 4.7 (a-b) Spherically averaged scaled correlation  $C(r, t)$  vs.  $r/R(t)$  and corresponding structure factor  $S(k, t)$  vs.  $kR(t)$  are plotted for different time intervals with various symbols mentioned in the legends. The solid black line in (a) represents the zero crossing of correlation function. The structure factor curves follow Porod's law:  $S(k, t) \sim k^{-4}$  at  $k \rightarrow \infty$  represented by a solid black line with slope  $-4$ . (c) The characteristic length scale over time for case 1. The solid black line with slope  $1/3$  represents the diffusive growth at early times which saturates later. (d) Plots for the effective growth exponent  $\phi_{eff}$  vs.  $1/R(t)$  correspond to the length scale plotted in (c). The solid black line illustrates the reference value of  $\phi_{eff} \sim 1/3$  for early diffusive growth. . . . . 90
- 4.8 Morphology evolution of BCP melts system for case 2 for three different shear rates (a)  $\dot{\gamma} = 1.56 \times 10^{-3}$ , (b)  $\dot{\gamma} = 7.80 \times 10^{-3}$ , and (c)  $\dot{\gamma} = 1.56 \times 10^{-2}$ . The snapshots are taken at two different time intervals:  $t = 1.2 \times 10^2$  (first column) and  $t = 5.4 \times 10^3$  (second column). The direction of the wall motion is shown with a magenta arrow. In the third column, the isosurfaces are plotted, corresponding to the evolution shown in the second column. . . . . 92

- 4.9 (a) and (b) represents the plots of  $g_{AB}(r)$  vs.  $r$  and  $\rho(y)$  of  $A$ -beads along  $y$ -direction, respectively for case 2. These data sets are computed at a fixed shear rate of  $\dot{\gamma} = 7.80 \times 10^{-3}$  for different time intervals mentioned in the legends. (c)  $g_{AB}(r)$  vs.  $r$  for different shear rates at a fixed time interval of  $t = 5.4 \times 10^3$ . (d)  $\rho(y)$  versus  $y$  for the same data set as in (c). 93
- 4.10 The characterization functions are plotted at a fixed time step  $t = 5.4 \times 10^3$  for different shear rates for case 2. The scaled correlation function  $C(r, t)$  versus  $r/R(t)$  is displayed in (a), While the corresponding structure factor  $S(k, t)$  versus  $kR(t)$  on a logarithmic scale is shown in (b). (c) The characteristic length scale is plotted against time for given shear rates. To calculate the growth exponent, we display the  $\phi_{eff}$  as a function of  $1/R(t)$  in (d). . . . . 95
- 4.11 The evolution snapshots for case 3, where both walls move in the same direction. Snapshots are plotted at two-time steps  $t = 1.2 \times 10^2$  and  $t = 5.4 \times 10^3$ . The shear rates applied to the system is varied as: (a)  $\dot{\gamma} = 1.56 \times 10^{-3}$ , (b)  $\dot{\gamma} = 7.80 \times 10^{-3}$ , and (c)  $\dot{\gamma} = 1.56 \times 10^{-2}$ . The third column represents the isosurfaces corresponding to the snapshots in the second column. The magenta arrows display the shear direction. . . . . 97
- 4.12 Case 3: Both walls are moving in  $x$ -direction with similar velocities. (a) Plots the  $g_{AB}(r)$  versus  $r$ , and (b) the average number density profiles of  $A$ -type beads in  $y$ -direction at  $t = 5.4 \times 10^3$  for different shear rates; related morphologies are shown in Fig. (4.11) . . . . . 98

- 4.13 (a) Spherically averaged  $C(r, t)$  vs.  $r/R(t)$  for different shear rates; related morphologies are illustrated in Fig. 4.11. The corresponding  $S(k, t)$  versus  $kR(t)$  curves are plotted in (b) on a log-log scale. (c)  $R(t)$  versus  $t$  for different shear rates. (d) Plots for related effective growth exponents  $\phi_{eff}$  versus  $1/R(t)$ . . . . . 99
- 4.14 Plots for the unidirectional structure factor  $S(k_x, k_y, k_z)$  versus  $k_y$  (black curve) and  $k_z$  (red curve) to discuss the structural anisotropy in the system. The data is calculated at a fixed shear rate of  $\dot{\gamma} = 7.80 \times 10^{-3}$  and plotted for case 2 in (a) while for case 3 in (b). The inset represents the  $S(k_x, k_y, k_z)$  versus  $k_y$  along diagonal and cross-diagonal directions with green and blue curves, respectively, in  $yz$ -plane. . . . . 100
- 4.15 Case 4: The evolution snapshots at two different time steps  $t = 1.2 \times 10^2$  and  $t = 5.4 \times 10^3$  for different shear rates (a)  $\dot{\gamma} = 1.56 \times 10^{-3}$ , (b)  $\dot{\gamma} = 7.80 \times 10^{-3}$ , and (c)  $\dot{\gamma} = 1.56 \times 10^{-2}$ . To see the bulk structures, we have plotted the isosurfaces in column three corresponding to the snapshots at  $t = 5.4 \times 10^3$ . . . . . 102
- 4.16 Case 4: (a) Comparison of  $g_{AB}(r)$  versus  $r$ , (b)  $\rho(y)$  versus  $y$  of  $A$ -type beads, (c)  $C(r, t)$  versus  $r/R(t)$ , and (d)  $S(k, t)$  versus  $kR(t)$  at  $t = 5.4 \times 10^3$  for different shear rates mentioned in the legends. (e) The characteristic average domain size  $R(t)$  vs.  $t$  for the evolution displayed in Fig. 4.15. (f) Plots for the effective growth exponents  $\phi_{eff}$  vs.  $1/R(t)$  for different shear rates. . . . . 103
- 4.17 We plot the unidirectional structure factor  $S(k_x, k_y, k_z)$  versus  $k_y$  (black curve) and  $k_z$  (red curve) for different shear rates of  $\dot{\gamma} = 0.0$  in (a),  $\dot{\gamma} = 1.56 \times 10^{-3}$  in (b),  $\dot{\gamma} = 7.80 \times 10^{-3}$  in (c), and  $\dot{\gamma} = 1.56 \times 10^{-2}$  in (d) to analyze the structural anisotropy developed in the system. . . . . 106

- 4.18 Time variation of anisotropy parameters,  $D_{xy}$ ,  $D_{yz}$ , and  $D_{xz}$  are plotted in (a-d). (a) represent the reference case 1 ( $\dot{\gamma} = 0.0$ ). (b-d) plots the same data for case 2 for different shear rates,  $\dot{\gamma} = 1.56 \times 10^{-3}$ ,  $7.80 \times 10^{-3}$ , and  $1.56 \times 10^{-2}$ , respectively. Time variations of  $D_{yz}$  are compared in (e) and (f) for case 3 and case 4 at different shear rates depicted by various symbol types. . . . . 107
- 4.19 Effect of shear on the BCP melt system with a smaller chain length of  $A_4B_4$ . We plot the late time evolution, and related isosurfaces of BCP melt for all three scenarios 2-4 at a fixed moderate shear rate of  $\dot{\gamma} = 7.80 \times 10^{-3}$  and time step  $t = 5.4 \times 10^3$ . Corresponding snapshots for  $\dot{\gamma} = 0.0$  is shown in Fig. 4.5(a). . . . . 108
- 4.20 The evolution snapshots and related isosurfaces for a BCP melt system with a smaller chain length of  $A_8B_8$ . The shear is applied with cases 2-4 with a moderate shear rate of  $\dot{\gamma} = 7.80 \times 10^{-3}$  and time step  $t = 5.4 \times 10^3$ . Corresponding snapshots for  $\dot{\gamma} = 0.0$  is shown in Fig. 4.5(b). . . . . 109
- 4.21 Domain evolution for asymmetric BCP melt system confined between two parallel rigid walls. (a) Evolution snapshot and related isosurface plot of BCP melt system with the ratio of 1:3 between  $A$  and  $B$  beads, at the time step  $t = 5.4 \times 10^3$  for zero shear rate. (b) Snapshot at the same time and zero shear for the BCP melt system with a 1:7 ratio of  $A$  and  $B$  beads. 110
- 4.22 Comparison of the effect of shear in different cases 2-4 in BCP melt system with 1:3 ratio of  $A$  and  $B$  beads. The evolution snapshots are taken at two different time intervals plotted in the first two columns at  $t = 1.2 \times 10^2$  and  $t = 5.4 \times 10^3$ , respectively. The third column plots the isosurface related to the snapshots at the late time. . . . . 111

- 4.23 Evolution snapshots of BCP melt system with 1:7 ratio of  $A$  and  $B$  beads for cases 2-4. The first two columns represent the morphology at  $t = 1.2 \times 10^2$  and  $t = 5.4 \times 10^3$ , respectively. The third column depicts the isosurface corresponding to the evolution shown in column two. . . . 112
- 5.1 (a) Variation of average velocity profile  $\langle v_x \rangle$  along  $z$ -direction for all cases mentioned in the legends. The data is plotted for a fixed shear rate  $\dot{\gamma} = 1.56 \times 10^{-2}$  at  $t = 1.2 \times 10^3$ . (b) Comparison of shear viscosity  $\langle \eta \rangle$  as a function of  $\dot{\gamma}$  at  $t = 1.2 \times 10^3$ . (c-e)  $\langle v_x \rangle$  vs.  $z$  for different shear rates for cases 2-4, respectively. . . . . 121
- 5.2 The evolution snapshots are shown at  $t = 0$  in (a) and  $t = 1.2 \times 10^3$  in (b); the red, yellow, and olive colors represent the  $A$ ,  $B$ , and wall-type beads, respectively. (c) The spatial intensity variation of  $S(k_x, k_z)$  at  $t = 1.2 \times 10^3$  along  $xz$ -plane. . . . . 123
- 5.3 (a) The RDF  $g_{AB}(r)$  vs.  $r$  is compared at different time steps for zero shear rate. (b) The scaled correlation function  $C(r, t)$  vs.  $r/R(t)$ . The solid black line represents the zero crossing. (c) The characteristic domain growth  $R(t)$  against time is plotted after averaging along  $x$ ,  $y$ , and  $z$  directions, as shown in the legends. The inset figure represents the spherically averaged length scale,  $R(t)$  vs.  $t$ . Solid black lines with slopes 1 and  $2/3$  represent the viscous and inertial hydrodynamic growth laws. (d) The unidirectional structure factor  $S(k_x, k_y, k_z)$  as a function of  $k_x$ ,  $k_y$ , and  $k_z$ . The inset correspond to  $S(k_x, k_y, k_z)$  vs.  $k_y$  along diagonal and cross-diagonal directions. . . . . 124

- 5.4 (a-c) The evolution snapshots and corresponding  $xz$ -cross section are displayed for case 2 with different shear rates: (a)  $\dot{\gamma} = 1.56 \times 10^{-2}$ , (b)  $\dot{\gamma} = 7.80 \times 10^{-3}$ , and (c)  $\dot{\gamma} = 1.56 \times 10^{-3}$ . Related isosurfaces are also provided in the inset of (d). (d) and (e) show  $C(r, t)$  vs.  $r/R(t)$  and  $R(t)$  vs.  $t$ , respectively, for different shear rates at  $t = 1.2 \times 10^3$ . The solid black lines in (e) represent the growth laws followed by  $R(t)$ . . . . . 126
- 5.5 The evolution snapshots for case 3 and corresponding  $xz$ -cross-section plots at  $t = 1.2 \times 10^3$  is displayed in (a-c) with different shear rates mentioned alongside them. Related isosurfaces are also provided in the inset of (d). Data for  $C(r, t)$  vs.  $r/R(t)$  and  $R(t)$  vs.  $t$  are plotted in (d) and (e), respectively, for different shear rates shown in the legends at  $t = 1.2 \times 10^3$ . The solid black lines in (e) represent the growth laws followed by  $R(t)$ . . . 128
- 5.6 (a-c) The evolution morphology and corresponding  $xz$ -cross section plots for the middle layer ( $y = 32$ ). These are the snapshots at the late time intervals  $t = 1.2 \times 10^3$  for different shear rates mentioned alongside them. (d)  $g_{AB}(r)$  vs.  $r$  for different  $\dot{\gamma}$  values. Inset represents the isosurfaces corresponding to the evolution pictures given in (a-c). (e)  $C(r, t)$  vs.  $r/R(t)$  is plotted for the same data set as in (d). The respective plots for  $R(t)$  vs.  $t$  averaged along the radial direction are illustrated in the inset of (e). (f-g) The average length scale along different directions is plotted for various  $\dot{\gamma}$  values. Solid lines with slopes 1 and  $2/3$  represent the viscous and inertial hydrodynamic growth laws followed by the system. . . . . 129

- 5.7 (a-d) The spatial intensity variation of the structure factor  $S(k_x, k_z)$  along  $xz$ -plane for different  $\dot{\gamma}$  values at  $t = 1.2 \times 10^3$ . To see the structural anisotropy, the unidirectional structure factor  $S(k_x, k_y, k_z)$  vs.  $k_x$  (black curve),  $k_y$  (red curve), and  $k_z$  (green curve) is plotted in (e), (f), and (g) for  $\dot{\gamma} = 1.56 \times 10^{-3}$ ,  $7.80 \times 10^{-3}$ , and  $1.56 \times 10^{-2}$ , respectively. The magenta and blue curves demonstrate  $S(k_x, k_y, k_z)$  vs.  $k_y$  along diagonal and cross-diagonal directions. . . . . 132
- 5.8 The evolution snapshots are shown at  $t = 0$  in (a) and  $t = 1.2 \times 10^3$  in (b). (c) The spatial intensity variation of  $S(k_x, k_z)$  at  $t = 1.2 \times 10^3$  along  $xz$ -plane. . . . . 134
- 5.9 Off-critical polymer mixture with ratio  $A : B = 3 : 1$ : (a)  $g_{AB}(r)$  vs.  $r$  at various time steps mentioned in the legends. (b) Plots for  $C(r, t)$  vs.  $r/R(t)$  for the same data set used in (a). (c) Characteristic length scale  $R(t)$  vs.  $t$  is represented along different directions with various symbol types in the legends. Inset plots the time-dependent spherically averaged domain length. (d) Plots for  $S(k_x, k_y, k_z)$  as a function of  $k_x$ ,  $k_y$ , and  $k_z$ , representing the anisotropy along different directions. In the Inset, the magenta and blue curves plot  $S(k_x, k_y, k_z)$  vs.  $k_y$  along diagonal and cross diagonal directions on  $xz$ -plane. . . . . 134
- 5.10 (a-c) Domain evolution and  $2d$  cross-section plots along  $xz$ -plane for the case 2. These pictures are related to different shear rates mentioned at left for the late time  $t = 1.2 \times 10^3$ . Related isosurfaces are also plotted in the inset of (d). (d) Scaled correlation as a function of  $r/R(t)$  for the same case as in (a-c). The corresponding time-dependent average domain size is plotted in (e).  $R(t)$  curves follow the viscous and inertial hydrodynamic growth represented by solid black lines with slopes 1 and  $2/3$ , respectively. 136

- 5.11 (a-c) Evolution snapshots and corresponding  $xz$ -cross section plots for  $y = 32$  at  $t = 1.2 \times 10^3$ . Related isosurfaces are also shown in the inset of (d). (d) Comparison of Scaled correlation  $C(r, t)$  vs.  $r/R(t)$  corresponding to the evolutions plotted in (a-c). (e)  $R(t)$  vs.  $t$  for different shear rates mentioned in the legends. Solid black lines with slope 1 and  $2/3$  represent the growth laws followed by  $R(t)$ . . . . . 137
- 5.12 (a-c) Plots for the late-time domain evolution and corresponding  $xz$ -cross section plots for  $y = 32$  at different shear rates. (d) The RDF plots for different  $\dot{\gamma}$  values at  $t = 1.2 \times 10^3$ . Inset represents the isosurfaces corresponding to the evolution pictures displayed in (a-c). (e)  $C(r, t)$  vs.  $r/R(t)$  for different shear rates, same as in (d). A solid black line depicts zero crossing. Inset represents the plots for  $R(t)$  vs.  $t$  for different  $\dot{\gamma}$  values. (f-h)  $R(t)$  vs.  $t$  averaged along  $x$ ,  $y$ , and  $z$  directions for different shear rates given in each figure.  $R(t)$  curves show a cross-over from viscous to inertial hydrodynamic growth represented by solid lines. . . . . 139
- 5.13 (a-d) The intensity variation of the structure factor along  $xz$ -plane for different shear rates at  $t = 1.2 \times 10^3$ . Unidirectional structure factor  $S(k_x, k_y, k_z)$  vs.  $k_x$ ,  $k_y$ , and  $k_z$  is compared for  $\dot{\gamma} = 1.56 \times 10^{-3}$  in (e),  $\dot{\gamma} = 7.80 \times 10^{-3}$  in (f), and  $\dot{\gamma} = 1.56 \times 10^{-2}$  in (g) at  $t = 1.2 \times 10^3$ . The inset of each picture depict the variation of structure factor as a function of  $k_y$  along diagonal and cross-diagonal directions. . . . . 141
- 6.1 Phase separation kinetics of different systems inside hydrogel. . . . . 147
- 6.2 Mixing and de-mixing in the dimer melt system on the application of alternate on-off light cycles. . . . . 147